Journal of Alloys and Compounds 960 (2023) 170703

Contents lists available at ScienceDirect

Journal of Alloys and Compounds

journal homepage: www.elsevier.com/locate/jalcom

High-temperature wear behavior of a Zr-based metallic glass

Fei Sun [a,1], Xiangyang Yu [a,1], Jianan Fu [b], Youcheng Zhu [a], Wenxue Wang [a], Rongce Sun [a], Heting Zhang [a], Feng Gong [a], Jiang Ma [a,c,*], Jun Shen [a,c]

[a] State Key Laboratory of Radio Frequency Heterogeneous Integration, Shenzhen University, China
[b] Shenzhen Key Laboratory of Cross-scale Manufacturing Mechanics, Southern University of Science and Technology, Shenzhen 518055, China
[c] Shenzhen Key Laboratory of High Performance Nontraditional Manufacturing, College of Mechatronics and Control Engineering, Shenzhen University, Shenzhen 518060, China

ARTICLE INFO

Article history:
Received 18 March 2023
Received in revised form 21 May 2023
Accepted 22 May 2023
Available online 23 May 2023

Keywords:
High-temperature wear
Zr-based bulk metallic glass
Wear behavior
Mechanisms

ABSTRACT

Due to the fascinating application prospects of Zr-based bulk metallic glass (BMG), it is of practical engineering interest to study its wear behavior and mechanism under various temperature conditions. In this work, the wear behavior and mechanism of a commercially available $Zr_{35}Ti_{30}Be_{26.75}Cu_{8.25}$ BMG at room temperature (RT) to 500 °C were investigated. The results demonstrated that the wear rate increased from ~24.7×10^{-5} mm^3 N^{-1} m^{-1} to ~196.8×10^{-5} mm^3 N^{-1} m^{-1} as the temperature increased from RT to 500 °C. Accordingly, the coefficient of friction (COF) is reduced from an average of 0.45–0.18 due to the lubricating effect of the oxide layer. At low temperatures of RT and 200 °C, the predominant wear mechanisms are abrasive wear and adhesive wear. However, in the supercooled liquid region (SCLR) of at 350 °C, the dominant wear mechanism is a combination of superplasticity-dominated abrasive wear, severe fatigue wear, and slight oxidative wear. Above the crystallization temperature (T_x) at 500 °C, the primary wear mechanisms are severe abrasive wear and oxidative wear. Our results can provide important guidance for determining the applicable temperature, service life and failure mode of BMG components.

1. Introduction

Bulk metallic glasses (BMGs), are a cutting-edge type of material that has been gaining popularity in recent years due to their remarkable properties, such as exceptional strength, high hardness, and good wear resistance [1–7]. The superior performance of BMGs can be attributed to the rapid cooling technology that enables the preservation of the disordered atomic structure. They are a rising engineering material with a vast range of application potentials, including precision components, defense equipment, and sporting goods [8–12]. However, the limited glass forming ability (GFA) and inherent brittleness severely limit the practical engineering applications. To date, superior GFA is only found in a limited number of MG systems and the majority are precious metal-based [13–16]. Fortunately, in addition to precious metal-based BMGs, low-cost Zr-based BMG systems also exhibit excellent GFA and performance [17–19]. These alloys offer a more cost-effective option for those seeking the benefits of BMGs while avoiding the high costs typically associated with precious metal-based materials. As a result, Zr-based BMGs are becoming increasingly popular in a wide range of applications, offering an attractive alternative to traditional metallic materials.

In practical applications, components are often subjected to frequent friction and high-temperature conditions. Given the great application potential of Zr-based BMGs, it is crucial to investigate their temperature-dependent wear behavior and mechanisms. So far, many efforts have been devoted to studying the temperature-dependent wear behavior of Zr-based BMGs [7,20–23]. In a study conducted by Salehan [24] et al., the impact of various annealing states on the wear behavior of $Zr_{60}Cu_{10}Al_{15}Ni_{15}$ BMG was evaluated. The results reveal that relaxed samples exhibit optimal wear resistance and highlight the dependence of the material's wear resistance on the dominant wear mechanism during the wear process. Jin [25] et al. conducted an investigation on the impact of various annealing temperatures on the wear behavior of $Zr_{42}Ti_{15.5}Cu_{14.5}Ni_{3.5}Be_{24.5}$ BMG. The results show a gradual reduction in the wear rate as the annealing temperature

* Corresponding author at: State Key Laboratory of Radio Frequency Heterogeneous Integration, Shenzhen University, China.
E-mail address: majiang@szu.edu.cn (J. Ma).
[1] These authors contributed equally to this work.

https://doi.org/10.1016/j.jallcom.2023.170703
0925-8388/

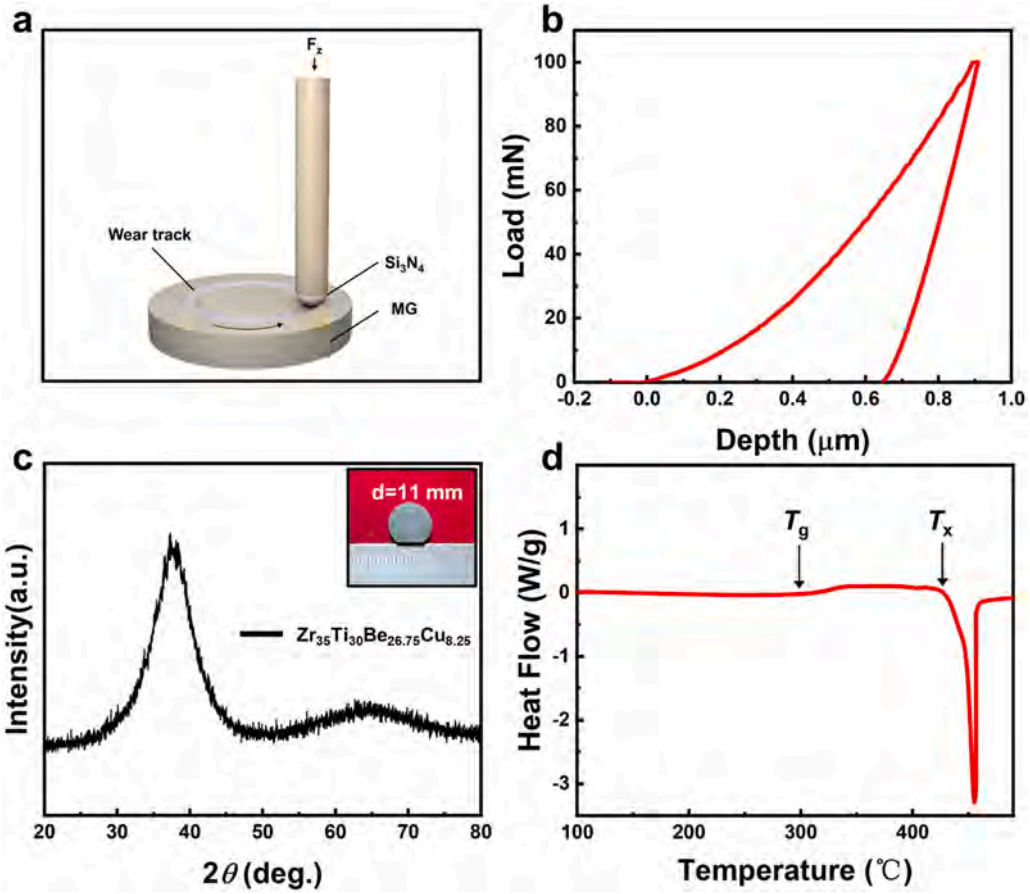

Fig. 1. (a) Schematic of the wear experiment. (b) Nanoindentation curve of the BMG specimen. (c) The XRD curve of primitive BMG samples, and the inset presents a photograph of a typical specimen. (d) The DSC curve of primitive BMG samples.

increased, with hardness playing a determining role in the wear rate. Wang [20] et al. conducted a study to investigate the wear behavior of $Zr_{55}Cu_{30}Al_{10}Ni_5$ BMG after oxidation treatment in the supercooled liquid region (SCLR). The findings suggest that the formation of surface oxides brought about a substantial enhancement in hardness, as evidenced by a twofold increase in hardness compared to cast samples. Additionally, there was a decrease of 40 % in the COF. Bajpai [22] et al. investigated the influence of different fictive temperatures on the wear behavior of $Zr_{44}Ti_{11}Cu_{10}Ni_{10}Be_{25}$ BMG. They found that as fictive temperature increased, hardness and effective elastic modulus decreased and there was more free volume, enhancing atomic and plastic flow in the material. And the samples with fictive temperature equal to 0.91 times the glass transition temperature (T_g) were the most wear resistant. Although many studies have reported the temperature-dependent tribological behavior of Zr-based BMGs, most of them were conducted at room temperature (RT) after pre-treatment below the T_g. To the best of the authors' knowledge, only a limited number of studies have explored the impact of real-time high-temperature conditions on the tribological behavior of Zr-based BMGs. Therefore, studying the wear behavior of Zr-based BMG under different temperature conditions, such as RT, below T_g, above T_g, and even above the crystallization temperature (T_x), is important for the life prediction and failure regimes of BMG components in practical applications.

In this work, the wear behavior and mechanism of a commercially available $Zr_{35}Ti_{30}Be_{26.75}Cu_{8.25}$ was investigated under different temperature conditions. In consideration of the potential harsh application environment, the wear temperatures were set to RT, 200 °C (below T_g), 350 °C (above T_g), and 500 °C (above T_x), respectively. The results show that the wear rate increases from ~24.7×10^{-5} mm^3 N^{-1} m^{-1} to ~196.8×10^{-5} mm^3 N^{-1} m^{-1} as the temperature increases from RT to 500 °C. And due to the lubricating effect of the oxides formed at high temperatures [20,26,27], the corresponding coefficient of friction (COF) is reduced from an average of 0.5–0.18. The main wear mechanisms at lower temperatures of RT and 200 °C, are abrasive wear and adhesive wear. When the temperature is set above T_g at 350 °C, the main wear mechanisms at this temperature are oxidative wear and abrasive wear characterized by significant plastic deformation. As the temperature rises to 500 °C, the wear rate is maximum. And the main wear mechanisms at this time are severe abrasive wear and oxidative wear. Our results are of great significance for determining the application scenarios where Zr-based BMG components are suitable and for predicting their service life.

2. Experimental

2.1. Sample preparation

The commercially available $Zr_{35}Ti_{30}Be_{26.75}Cu_{8.25}$ BMG plate with a thickness of 2 mm was purchased directly from Dongguan Yi'an Technology Co. For the convenience of the experiment, the BMG specimens were cut into 11 mm diameter disks using a low-speed wire electrical discharge machining (WEDM; SODICK AP250L). Prior to the wear experiments, the sample surfaces were successively polished with 400–3000 grits sandpapers and subsequently polished with a 0.1 μm diamond suspension.

2.2. Characterizations

The X-ray diffraction (XRD; Rigaku MiniFlex 600) with Cu Kα radiation was used to examine the glassy nature of BMG samples.

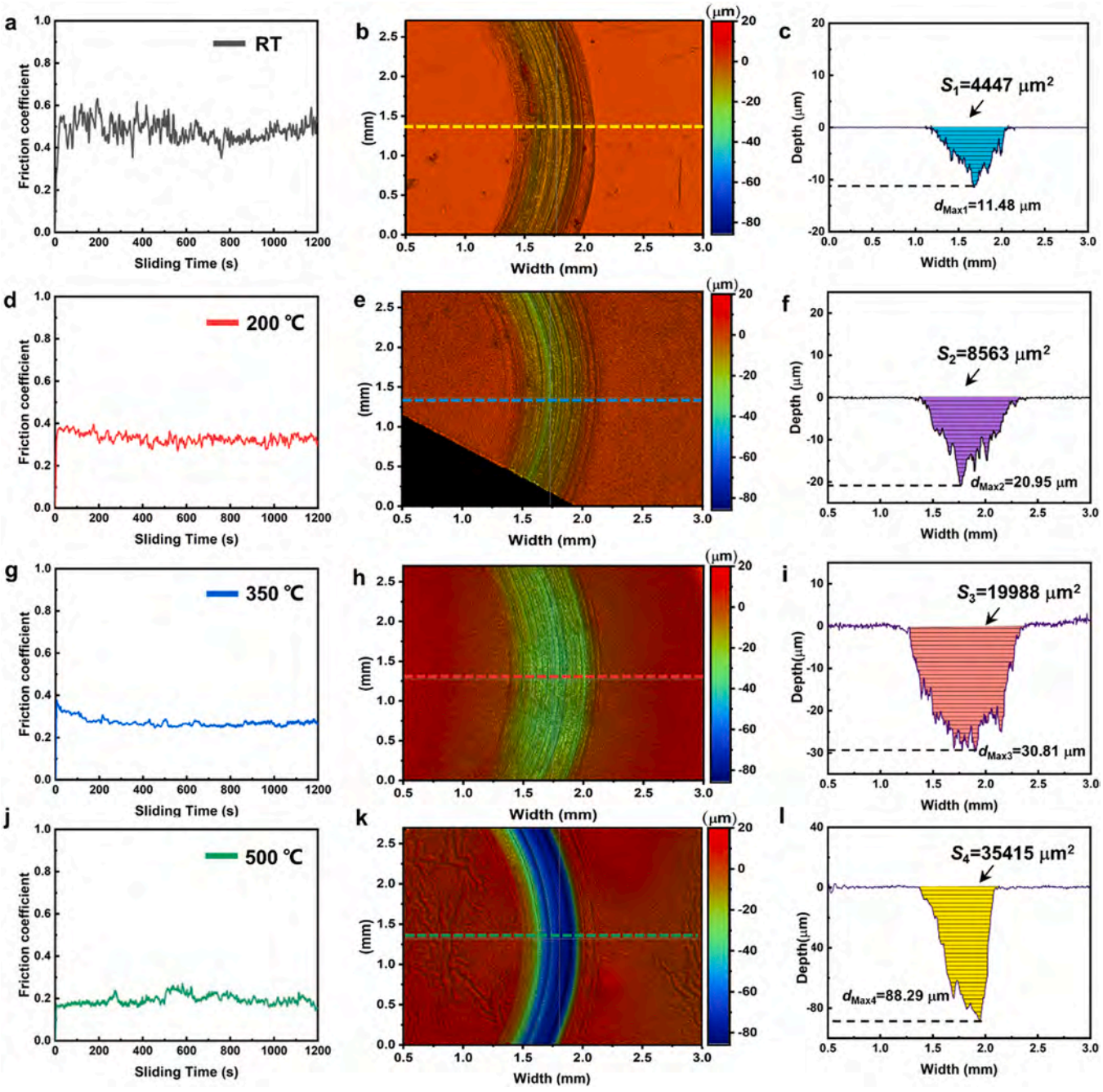

Fig. 2. (a-c) The COF curves, 3D morphology and cross-sectional shape of Zr-based BMG at RT. (d-f) The COF curves, 3D morphology and cross-sectional shape of Zr-based BMG at 200 °C. (g-i) The COF curves, 3D morphology and cross-sectional shape of Zr-based BMG at 350 °C. (j-m) The COF curves, 3D morphology and cross-sectional shape of Zr-based BMG at 500 °C.

The thermal properties of BMG samples were measured by differential scanning calorimetry (DSC; Perkin-Elmer DSC-8000) with a heating rate of 20 °C/min. The nanoindenter (TI750 Hysitron Ltd) was used to test the hardness and modulus of the BMG samples. The maximum load was 100 mN and the loading rate was 2500 μN/s. The morphology and elemental distribution of the wear traces after the wear experiments were analyzed using a field emission scanning electron microscope (SEM, FEI QUANTA FEG 450) equipped with an energy disperse spectroscopy (EDS) module. The volume loss and the depth of wear traces after wear experiments at different temperatures were evaluated using a white light interference profiler (Bruker ContourGT-X 3D).

2.3. Wear test

Dry sliding wear experiments were conducted on the top surface of BMG samples by using a ball-on-disk tribometer (Rtec MFT-5000, USA) under air atmosphere, the schematic is depicted in Fig. 1(a). Si_3N_4 balls with a diameter of 9.5 mm was selected as the counterpart material. The speed was fixed at a relatively slow 30 rpm/min to reduce the temperature rise caused by friction. In addition, a total sliding time of 20 min and a load of 30 N were applied to all wear tests. The value of COF is assessed by the steady state of its curve. The wear rate ω is obtained from the volume-loss equation [7,28,29]:

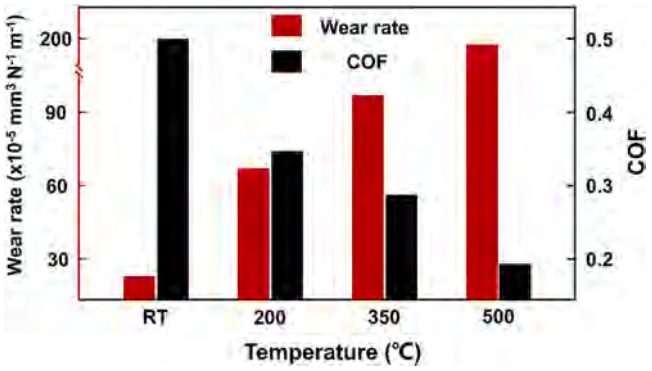

Fig. 3. Summary of the wear rate and COF of Zr-based BMG at different temperatures.

$$\omega = \frac{V_{loss}}{L^*P}, \quad (1)$$

Where V_{loss} is the total volume lost (mm^3), L is the total wear distance (m), which is calculated from the wear time (min), wear speed (rpm) and wear radius (mm), and P is the applied load (N).

3. Results and discussion

The hardness and modulus of original BMG samples were determined using nanoindentation, with a maximum load of 100 mN applied. The resulting load versus displacement curve is shown in Fig. 1(b). To ensure accuracy, 10 points were collected for each sample and the data was then averaged. The average hardness and modulus of the BMG were calculated to be 6.4 GPa and 111.3 GPa, respectively. Fig. 1(c) displays the XRD spectrum of the sample, which confirms the completely glassy structure of the original BMG sample. The inset in Fig. 1(c) shows a typical BMG sample before wear, and it is required to note that the notch is designed to fixture the sample. Fig. 1(d) displays the DSC results of the Zr-based BMG samples. From the results, it can be seen that T_g is approximately 298 °C, T_x is around 435 °C, and ΔT (= T_x-T_g) is calculated to be 137 °C.

3.1. Wear resistance different temperatures

Fig. 2(a) displays the COF depending on time of $Zr_{35}Ti_{30}Be_{26.75}Cu_{8.25}$ BMG at RT. One can find that the COF shows a sudden increase followed by a gradual decrease, which is referred to as the "running-in" stage and is related to the roughness of the surfaces that come into contact and undergo loading [30]. In the subsequent stable-wear stage, it can be found that the average COF between the BMG specimens and Si_3N_4 counterparts at RT is about 0.45. The three-dimensional (3D) morphology and the corresponding cross-sectional shape of the wear trace after wear at RT are shown in Fig. 2(b) and (c), respectively. Based on the cross-sectional profile presented in Fig. 2(c), we can find that the maximum depth (d_{Max1}) and cross-sectional area (S_1) of the wear trace are 11.48 μm and ~4447 μm^2, respectively. By the integration method, the corresponding wear rate (ω_1) at RT can be calculated to be $\sim 24.7 \times 10^{-5}$ mm^3 N^{-1} m^{-1}. As the temperature increases to 200 °C, a decrease in average COF from 0.45 to 0.35 and a relatively smoother trend can be observed (see Fig. 2(d)), which is considered to be caused by the lubricating effect of the oxide film formed at high temperatures [31]. And Fig. 2(e-f) show the 3D morphology and the corresponding cross-sectional shape of the wear trace after wear at 200 °C, respectively. We can find a further increase in wear with a cross-sectional area (S_2) of ~8563 μm^2, a maximum depth (d_{Max2}) of 20.95 μm and a corresponding wear rate (ω_2) of $\sim 71.2 \times 10^{-5}$ mm^3 N^{-1} m^{-1}.

At 350 °C, the BMG specimen experiences a glassy transition that leads to reduced hardness and viscosity [32,33]. This transition causes an even greater increase in the maximum depth and volume loss of the wear trace. As shown in Fig. 3(g-i), a further decrease in COF (about 0.28) can be observed, the maximum depth (d_{Max3}) and cross-sectional area (S_3) of 30.81 μm and ~19,988 μm^2, respectively, and a corresponding wear rate (ω_3) of $\sim 111.0 \times 10^{-5}$ mm^3 N^{-1} m^{-1}. At a wear temperature of 500 °C higher than T_x, the BMG specimen undergoes a gradual transformation into a crystalline structure. The crystallization

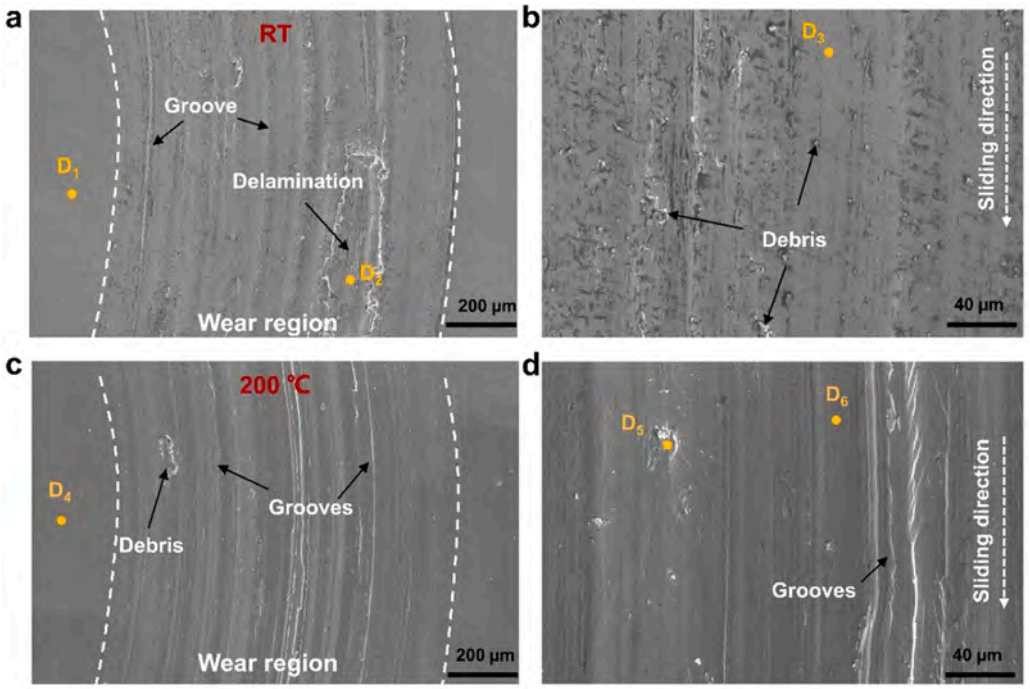

Fig. 4. (a-b) The wear morphology and magnification of Zr-based BMG at RT. (c-d) The wear morphology and magnification of Zr-based BMG at 200 °C.

Table 1
The statistics of elemental oxygen content in different regions (at RT, 200 °C).

Position Element	D_1	D_2	D_3	D_4	D_5	D_6
O (at%)	5.37	20.15	5.39	6.88	48.75	5.32

transformation caused the specimen to lose its exceptional properties and the corresponding COF curve, wear morphology is illustrated in Fig. 2(j-l). We can find that at 500 °C the COF decreases to about 0.18, the maximum depth (d_{Max4}) of wear trace is 88.29 μm, the area of the cross section (S_4) is ~35,415 μm^2 and the corresponding wear rate (ω_4) is ~196.8 × 10^{-5} mm^3 N^{-1} m^{-1}. For comparison, the trends of the wear rate and COF of Zr-based BMG with different temperature are visualized and plotted in Fig. 3. It can be found that as the temperature increases from RT to 350 °C, the wear rate gradually increases from ~24.7 × 10^{-5} mm^3 N^{-1} m^{-1} to ~111.0 × 10^{-5} mm^3 N^{-1} m^{-1}. This is caused by the fact that the hardness of the workpiece gradually decreases as the temperature increases, which is in accordance with Archard's law[23,34,35]. The dramatic increase in wear rate at 500 °C was caused by the crystallization of BMG and the loss of its original excellent properties. Accordingly, the gradual reduction of COF from about 0.5–0.18 is due to the lubricating effect possessed by the formation of oxide films at high temperatures [31].

3.2. Wear mechanism

Fig. 4(a-b) display the morphology and detailed features of the wear trace of Zr-based BMG after being worn at RT. Typical grooves, debris and delamination structures can be observed in the wear region, which indicates that the wear mechanism under RT contains abrasive wear and adhesive wear. In addition, the distribution of oxygen elements in different characteristic regions on the wear trace was analyzed using EDS (see Table 1). The oxygen content in the non-wear region (D_1) and inside the grooves (D_3) is 5.37 % and 5.39 %, respectively, which indicates that no significant oxidation occurred in these regions. It is noted that the oxygen content at the delamination structure (D_2) is 20.15 %, which indicates the attachment of oxides in this region. Therefore, the main wear mechanisms under RT are abrasive wear and adhesive wear. Furthermore, the wear morphology and details at 200 °C are shown in Fig. 4(c-d). As the temperature increases, more pronounced grooves can be found, which indicates that abrasive wear dominates the wear process. Similarly, the elemental oxygen content of the different characteristic regions after wear at 200 °C is also counted in Table 1. The oxygen content in the non-wear region (D_4) and inside the grooves (D_6) is only 6.88 % and 5.32 %, respectively, which can be attributed to the improved oxidation resistance provided by the Be element in the Zr-based BMG [18]. However, the oxygen content in the debris region (D_5) is up to 48.75 %, which proves the presence of adhesive wear of oxides during the wear process. Therefore, the main wear mechanism at 200 °C is a combination of more pronounced abrasive wear and adhesive wear, as well as slight oxidation wear.

The morphology and details of Zr-based BMG after wear in SLR (at 350 °C) are presented in Fig. 5(a-b). Firstly, one can notice the presence of numerous disorganized groove structures within the wear trace (see Fig. 5(a)). Interestingly, numerous "fold-like" structures can be found in the non-wear region (see details of Fig. 5(a)). The aforementioned characteristic morphology can be attributed to the unique superplasticity of BMG in SLR [36,37]. In Fig. 5(b), that shows more details, one can find a large amount of peeling and cracking, which reveals the characteristics of fatigue wear. In addition, the content of elemental oxygen in different characteristic regions was also detected. As summarized in Table 2, the oxygen content in non-wear region (D_7), in groove (D_8), in peeling region (D_9), and in crack region (D_{10}) is 23.23 %, 18.42 %, 21.64 %, 31.40 %, respectively. It indicates that oxidative wear is also one of the main wear mechanisms of Zr-based BMG at 350 °C. Therefore, we can conclude that the wear mechanism at 350 °C is a combination of superplasticity-driven abrasive wear, fatigue wear and oxidative wear.

Finally, the morphology of the Zr-based BMG workpiece after wear at 500 °C are shown in Fig. 6(a-b). Obviously, as the temperature increases to 500 °C, the dominant wear mechanism changes. Due to the set temperature exceeding T_x, the BMG gradually loses its disordered atomic structure and transforms into a crystal. As shown in Fig. 6(a), the organized and deeper groove structures created by abrasive wear are dispersed across the wear trace. Furthermore, different from the

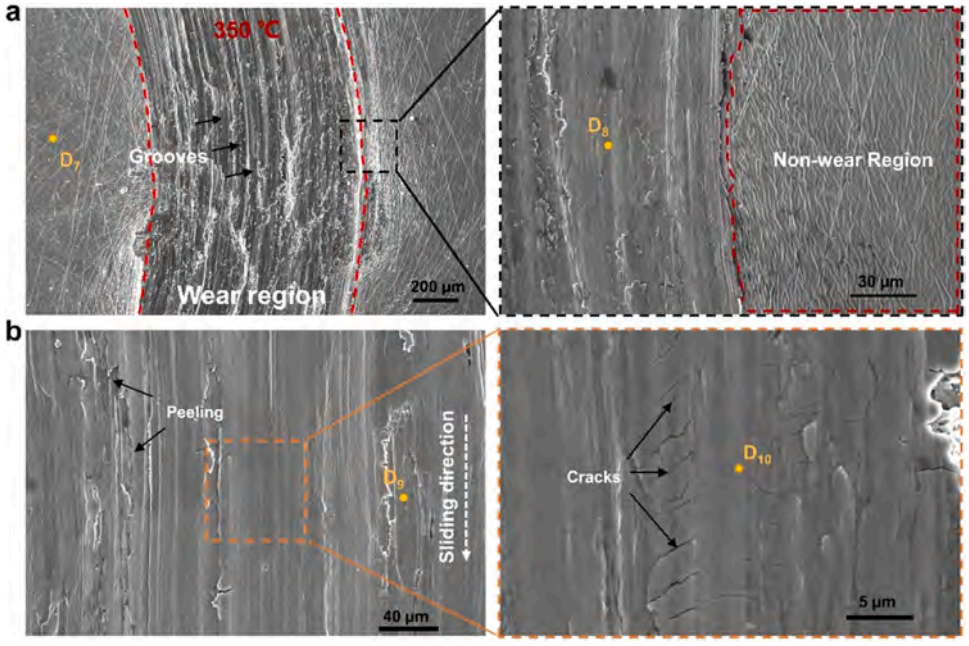

Fig. 5. (a-b) The wear morphology and magnification of Zr-based BMG at 350 °C.

Table 2
The statistics of elemental oxygen content in different regions (at 350 °C , 500 °C).

Position Element	D_7	D_8	D_9	D_{10}	D_{11}	D_{12}	D_{13}
O (at%)	23.23	18.42	21.64	31.40	58.36	54.26	49.46

wear morphology at RT and 200 °C, slight plastic deformation can be observed after wear at 500 °C, this is due to the recovery of plasticity after transformation to crystals. In the magnified view, significant peeling can be found, which implies that fatigue wear occurred. Similarly, the elemental oxygen content of different characteristic regions was detected. As shown in Table 2, the oxygen content in the non-wear region (D_{11}), in the groove (D_{12}), and in the exfoliated region (D_{13}) is up to 58.36 %, 54.26 %, and 49.46 %, respectively. It means that at 500 °C, the transformation of Zr-based BMG into crystals is accompanied by severe oxidation. Therefore, the predominant wear mechanisms of Zr-based BMG at 500 °C are a combination of abrasive wear, oxidative wear, and fatigue wear.

The wear behavior and mechanisms of $Zr_{35}Ti_{30}Be_{26.75}Cu_{8.25}$ BMGs vary depending on the temperature conditions. To facilitate understanding, the structural state and the major wear mechanism of the BMG at different temperatures are illustrated in Fig. 7. At lower temperatures of RT and 200 °C, the BMG maintains its original disordered structure. Therefore, the high hardness of the BMG dominates the wear process, and the main wear mechanisms are minor abrasive wear and adhesive wear of oxides. As the temperature rises above T_g

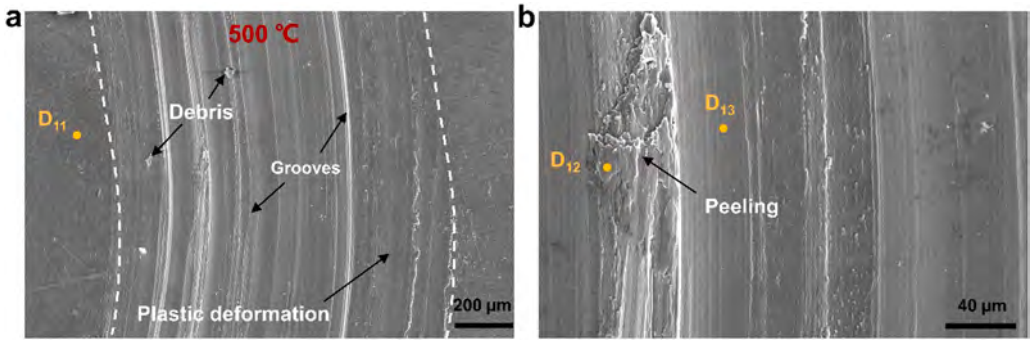

Fig. 6. (a-b) The wear morphology and magnification of Zr-based BMG at 500 °C.

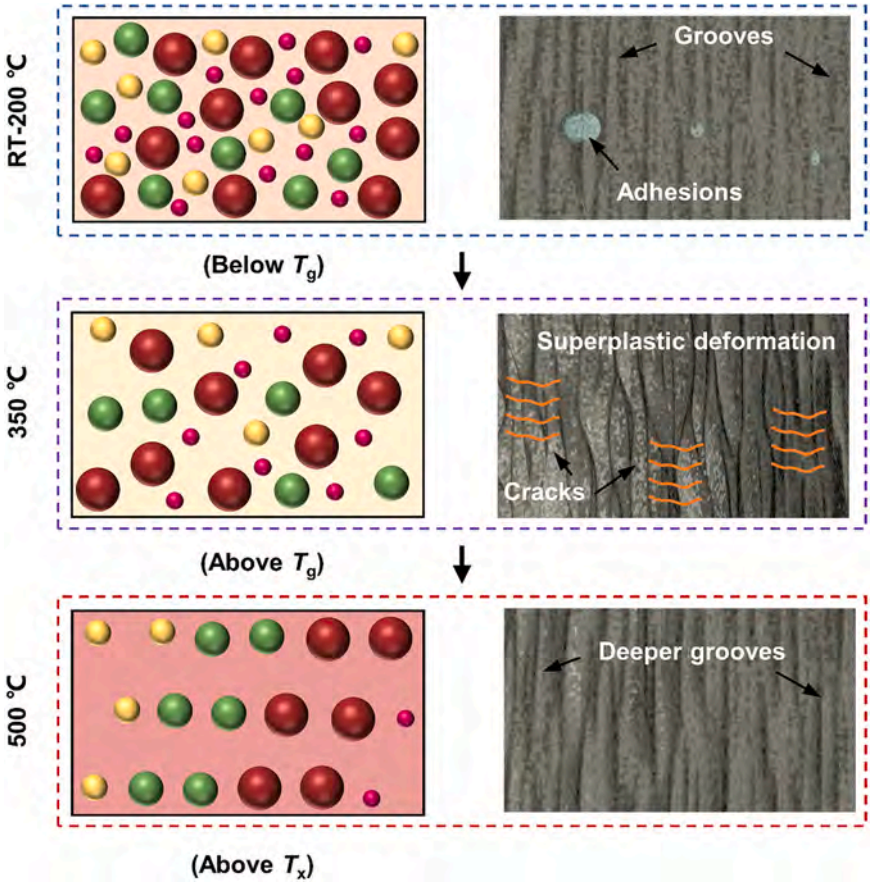

Fig. 7. Schematic of the wear mechanism of $Zr_{35}Ti_{30}Be_{26.75}Cu_{8.25}$ BMG at different temperatures.

(at 350 °C), due to the thermal expansion of BMG, the atoms inside it become loose. Meanwhile, the BMG experiences the glass transition resulting in a dramatic decrease in viscosity and superplasticity. Thus, the primary wear mechanisms at 350 °C is plasticity-dominated abrasive wear, and accompanied by significant fatigue wear. As the temperature rises above T_x (at 500 °C), BMG undergoes crystallization into crystals, while the internal atoms become more loosely packed. Due to the loss of amorphous structure, the hardness of BMG decreases and plasticity increases. In addition, severe oxidation occurred due to the increase in temperature. Therefore, the prevailing wear mechanisms at 500 °C are significant oxidative wear, abrasive wear and some plastic deformation.

4. Conclusions

In conclusion, we investigated the wear behavior and mechanism of $Zr_{35}Ti_{30}Be_{26.75}Cu_{8.25}$ BMG depending on different temperatures. Since the temperature increases from RT to 500 °C, the wear resistance of BMG gradually decreases and the wear rate increases from $\sim 24.7 \times 10^{-5}$ mm^3 N^{-1} m^{-1} to $\sim 196.8 \times 10^{-5}$ mm^3 N^{-1} m^{-1}. Meanwhile, the average COF gradually decreases from 0.45 to 0.18 due to the lubricating effect of the oxides formed at high temperatures. At RT and 200 °C (below T_g), abrasive wear and adhesive wear are the dominant wear mechanisms. At 350 °C (above T_g), the unique superplasticity of BMG governed the wear process. Disorganized grooves in the wear region and fold-like structures in the non-wear region are the main wear characteristics. In addition, extensive cracking and peeling were observed, which reveals the presence of fatigue wear at this temperature. At 500 °C (above T_x), more severe abrasive wear and oxidative wear are the main wear mechanisms of the wear process due to the transition from amorphous to crystalline structure.

CRediT authorship contribution statement

Fei Sun: Methodology, Validation, Formal Analysis, Investigation, Data curation, Writing-Original Draft, Visualization**. Xiangyang Yu**: Investigation, Methodology, Validation, Data curation**. Jianan Fu**: Methodology, Investigation**. Youcheng Zhu**: Investigation, Methodology**. Wenxue Wang**: Investigation, Methodology**. Rongce Sun**: Investigation, Methodology**. Heting Zhang**: Investigation, Methodology**. Feng Gong**: Editing, Supervision**. Jiang Ma**: Writing-Review & Editing**,** Supervision**. Jun Shen:** Writing Review & Editing, Supervision.

Data availability

Data will be made available on request.

Declaration of Competing Interest

The authors declare that they have no known competing financial interests or personal relationships that could have appeared to influence the work reported in this paper.

Acknowledgments

The work was supported by the National Key Research and Development Program of China (Grant No. 2018YFA0703605), the Key Basic and Applied Research Program of Guangdong Province, China (Grant Nr. 2019B030302010), the NSF of China (Grant Nr. 52122105, 51971150) the Science and Technology Innovation Commission Shenzhen (Grants No. 20220804091920001). The authors also thank the assistance on microscope observation received from the Electron Microscope Center of the Shenzhen University. In addition, we appreciate eceshi (www.eceshi.com) for the SEM and EDS analysis.

References

[1] A.L. Greer, Metallic glasses, Science 31 (1995) 1947–1953, https://doi.org/10.1126/science.267.5206.1947
[2] W. Klement, R.H. Willens, P. Duwez, Pol, Non-crystalline structure in solidified gold–silicon alloys, Nature 187 (1960) 869–870.
[3] F. Sun, B. Wang, F. Luo, Y.Q. Yan, H.B. Ke, J. Ma, J. Shen, W.H. Wang, Shear punching of bulk metallic glasses under low stress, Mater. Des. 190 (2020) 108595, https://doi.org/10.1016/j.matdes.2020.108595
[4] F. Sun, J. Yang, J. Fu, B. Wang, J. Ma, J. Shen, Hierarchical macro to nano press molding of optical glasses by using metallic glasses, J. Non-Cryst. Solids 594 (2022) 121821, https://doi.org/10.1016/j.jnoncrysol.2022.121821
[5] F. Sun, S. Deng, J. Fu, J. Zhu, D. Liang, P. Wang, H. Zhao, F. Gong, J. Ma, Y. Liu, J. Shen, Superior high-temperature wear resistance of an Ir-Ta-Ni-Nb bulk metallic glass, J. Mater. Sci. Technol. 158 (2023) 121–132, https://doi.org/10.1016/j.jmst.2023.02.040
[6] A.H. Cai, G. Zhou, P.W. Li, D.W. Ding, Q. An, G.J. Zhou, Q. Yang, Y.P. Lin, H. Mao, Mechanical properties for a series of Zr-based bulk metallic glasses, J. Alloy. Compd. 938 (2023) 168579, https://doi.org/10.1016/j.jallcom.2022.168579
[7] Q. Zhou, W. Han, D. Luo, Y. Du, J. Xie, X.-Z. Wang, Q. Zou, X. Zhao, H. Wang, B.D. Beake, Mechanical and tribological properties of Zr–Cu–Ni–Al bulk metallic glasses with dual-phase structure, Wear 474-475 (2021) 203880, https://doi.org/10.1016/j.wear.2021.203880
[8] M.M. Khan, A. Nemati, Z.U. Rahman, U.H. Shah, H. Asgar, W. Haider, Recent advancements in bulk metallic glasses and their applications: a review, Crit. Rev. Solid State Mater. Sci. 43 (2017) 233–268, https://doi.org/10.1080/10408436.2017.1358149
[9] E. Axinte, Metallic glasses from “alchemy” to pure science: present and future of design, processing and applications of glassy metals, Mater. Des. 35 (2012) 518–556, https://doi.org/10.1016/j.matdes.2011.09.028
[10] M. Chen, A brief overview of bulk metallic glasses, NPG Asia Mater. 3 (2011) 82–90, https://doi.org/10.1038/asiamat.2011.30
[11] A. Inoue, A. Takeuchi, Recent development and application products of bulk glassy alloys, Acta Mater. 59 (2011) 2243–2267, https://doi.org/10.1016/j.actamat.2010.11.027
[12] Tao Xiang Peng Du, G.Xie Zeyun Cai, The influence of porous structure on the corrosion behavior and biocompatibility of bulk Ti-based metallic glass, J. Alloy. Compd. 906 (2022) 164326, https://doi.org/10.1016/j.jallcom.2022.164326
[13] N. Nishiyama, K. Takenaka, H. Miura, N. Saidoh, Y. Zeng, A. Inoue, The world’s biggest glassy alloy ever made, Intermetallics 30 (2012) 19–24, https://doi.org/10.1016/j.intermet.2012.03.020
[14] Z.P. Lu, H. Bei, C.T. Liu, Recent progress in quantifying glass-forming ability of bulk metallic glasses, Intermetallics 15 (2007) 618–624, https://doi.org/10.1016/j.intermet.2006.10.017
[15] J. Schroers, Highly processable bulk metallic glass-forming alloys in the Pt–Co–Ni–Cu–P system, Appl. Phys. Lett. 84 (2004) 3666–3668, https://doi.org/10.1063/1.1738945
[16] M.X. Li, S.F. Zhao, Z. Lu, A. Hirata, P. Wen, H.Y. Bai, M. Chen, J. Schroers, Y. Liu, W.H. Wang, High-temperature bulk metallic glasses developed by combinatorial methods, Nature 569 (2019) 99–103, https://doi.org/10.1038/s41586-019-1145-z
[17] T.Zhang Akihisa Inoue, Fabrication of bulk glassy Zr55Al10Cu30Ni5 alloy of 30 mm in diameter by a suction casting method, Mater. Trans. JIM 37 (1996) 185–187, https://doi.org/10.2320/matertrans1989.37.185
[18] G. Duan, A. Wiest, M.L. Lind, J. Li, W.-K. Rhim, W.L. Johnson, Bulk metallic glass with benchmark thermoplastic processability, Adv. Mater. (2007) 4272–4275, https://doi.org/10.1002/adma.200700969
[19] J. Zhu, W. Gao, S. Cheng, X. Liu, X. Yang, J. Tian, J. Ma, J. Shen, Improving the glass forming ability and plasticity of ZrCuNiAlTi metallic glass by substituting Zr with Sc, J. Alloy. Compd. 909 (2022) 164679, https://doi.org/10.1016/j.jallcom.2022.164679
[20] M. Zhang, D. Yao, Z. Cao, P. Li, P. Zhou, X. Wang, Influence of oxidation on the performance of Zr55Cu30Al10Ni5 BMG, Intermetallics 79 (2016) 20–27, https://doi.org/10.1016/j.intermet.2016.08.007
[21] Q. Jia, W. He, D. Hua, Q. Zhou, Y. Du, Y. Ren, Z. Lu, H. Wang, F. Zhou, J. Wang, Effects of structure relaxation and surface oxidation on nanoscopic wear behaviors of metallic glass, Acta Mater. 232 (2022) 117934, https://doi.org/10.1016/j.actamat.2022.117934
[22] S. Bajpai, A. Nisar, R.K. Sharma, U.D. Schwarz, K. Balani, A. Datye, Effect of fictive temperature on tribological properties of Zr44Ti11Cu10Ni10Be25 bulk metallic glasses, Wear 486-487 (2021) 204075, https://doi.org/10.1016/j.wear.2021.204075
[23] M.R. Jones, A.B. Kustas, P. Lu, M. Chandross, N. Argibay, Environment-dependent tribological properties of bulk metallic glasses, Tribol. Lett. 68 (2020) 1–11, https://doi.org/10.1007/s11249-020-01364-z
[24] R. Salehan, H.R. Shahverdi, R. Miresmaeili, Effects of annealing on the tribological behavior of Zr60Cu10Al15Ni15 bulk metallic glass, J. Non-Cryst. Solids 517 (2019) 127–136, https://doi.org/10.1016/j.jnoncrysol.2019.05.013
[25] H.W. Jin, R. Ayer, J.Y. Koo, R. Raghavan, U. Ramamurty, Reciprocating wear mechanisms in a Zr-based bulk metallic glass, J. Mater. Res. 22 (2011) 264–273, https://doi.org/10.1557/jmr.2007.0048
[26] G. Jin, Z. Cai, Y. Guan, X. Cui, Z. Liu, Y. Li, M. Dong, D. zhang, High temperature wear performance of laser-cladded FeNiCoAlCu high-entropy alloy coating, Appl. Surf. Sci. 445 (2018) 113–122, https://doi.org/10.1016/j.apsusc.2018.03.135

[27] J. Cheng, J. Yang, X. Zhang, H. Zhong, J. Ma, F. Li, L. Fu, Q. Bi, J. Li, W. Liu, High temperature tribological behavior of a Ti-46Al-2Cr-2Nb intermetallics, Intermetallics 31 (2012) 120–126, https://doi.org/10.1016/j.intermet.2012.06.013
[28] T. Eyre, Wear characteristics of metals, Tribol. Int. 9 (1976) 203–212, https://doi.org/10.1016/0301-679X(76)90077-3
[29] A. Caron, P. Sharma, A. Shluger, H.J. Fecht, D.V. Louzguine-Luzguin, A. Inoue, Effect of surface oxidation on the nm-scale wear behavior of a metallic glass, J. Appl. Phys. 109 (2011) 083515, https://doi.org/10.1063/1.3573778
[30] Y. Sun, Y. Huang, H. Fan, F. Liu, J. Shen, J. Sun, J.J.J. Chen, Comparison of mechanical behaviors of several bulk metallic glasses for biomedical application, J. Non-Cryst. Solids 406 (2014) 144–150, https://doi.org/10.1016/j.jnoncrysol.2014.09.021
[31] K. Zhou, C. Chen, Y. Liu, S. Pang, N. Hua, W. Yang, T. Zhang, Effects of lutetium addition on formation, oxidation and tribological properties of a Zr-based bulk metallic glass, Intermetallics 90 (2017) 81–89, https://doi.org/10.1016/j.intermet.2017.07.007
[32] J. Schroers, Processing of bulk metallic glass, Adv. Mater. 22 (2010) 1566–1597, https://doi.org/10.1002/adma.200902776
[33] N. Li, Y. Chen, M.Q. Jiang, D.J. Li, J.J. He, Y. Wu, L. Liu, A thermoplastic forming map of a Zr-based bulk metallic glass, Acta Mater. 61 (2013) 1921–1931, https://doi.org/10.1016/j.actamat.2012.12.013
[34] J. Luo, W. Sun, D. Liang, K.C. Chan, X.-S. Yang, F. Ren, Superior wear resistance in a TaMoNb compositionally complex alloy film via in-situ formation of the amorphous-crystalline nanocomposite layer and gradient nanostructure, Acta Mater. 243 (2023) 118503, https://doi.org/10.1016/j.actamat.2022.118503
[35] S. Barlemont, P. Laffont, R. Daudin, A. Lenain, G. Colas, P.-H. Cornuault, Strong dependency of the tribological behavior of CuZr-based bulk metallic glasses on relative humidity in ambient air, Friction 11 (2023) 785–800, https://doi.org/10.1007/s40544-022-0680-z
[36] J. Schroers, The superplastic forming of bulk metallic glasses, JOM 57 (2005) 35–39, https://doi.org/10.1007/s11837-005-0093-2
[37] F. Sun, H. Lin, J. Fu, Z. Li, F. Luo, B. Wang, W. Ruan, S. Ren, Z. Zhang, X. Liang, J. Ma, J. Shen, Metallic glass based composites with precise tunable thermal expansion, Appl. Mater. Today 29 (2022) 101565, https://doi.org/10.1016/j.apmt.2022.101565